Journal of Materials Chemistry C

ROYAL SOCIETY OF CHEMISTRY

PAPER

View Article Online
View Journal | View Issue

Cite this: J. Mater. Chem. C, 2023, 11, 3826

Reaching the 5% theoretical limit of fluorescent OLEDs with push–pull benzophospholes†

Nicolas Ledos,[a] Denis Tondelier,[b] Bernard Geffroy,[c] Denis Jacquemin,*[de] Pierre-Antoine Bouit*[a] and Muriel Hissler*[a]

Received 20th January 2023,
Accepted 10th February 2023

DOI: 10.1039/d3tc00245d

rsc.li/materials-c

We report the synthesis and characterization of benzophosphole oxides featuring an ethoxy substituent on the P atom and electro-donating amino groups on the lateral phenyl groups. The optical and redox properties of these compounds are studied experimentally and computationally (TD-DFT). In particular, we show how the nature of the donor allows fine-tuning the internal charge transfer (ICT) and, thus, the optical properties. Considering the intense fluorescence in the solid state (powder or thin film) and the favorable redox and thermal properties, these compounds were introduced in multilayered organic light emitting devices. All compounds display high efficiency and one compound even exhibits an external quantum efficiency (EQE) of 5%, which represents the theoretical limit of the EQE of purely fluorescent emitters. These results highlight the potential of this novel family of fluorophores to develop next generation optoelectronic/photonic devices.

Introduction

Organic light-emitting diodes (OLEDs) are optoelectronic devices that convert electricity into light. Since their development in the late 80s,[1] they represent a sustainable lightning technology and have been applied to various displays (screens and phones) and lightning panels.[2] The first generation of OLEDs was based on fluorescent emitters. This technology allowed the field to rapidly expand but suffered from its intrinsic internal quantum efficiency (IQE) limit of 25%. This limit was then overcome with the use of phosphorescent emitters or thermally activated delayed fluorescent emitters (IQE = 100%). These two technologies now represent the benchmark for OLED devices. However, the combination of fluorescent emitters with a TADF assisted dopant (the so called TADF sensitized fluorescence TSF) appears as an elegant alternative to produce efficient OLEDs with high color purity.[3] In addition, purely fluorescent electroluminescent materials are also expected to have great potential in the field of electrically pumped organic lasers, where triplet states are highly detrimental,[4] or in visible light communications (VLC) that need an ultrafast response excluding the use of triplet emitters (or TADF).[5] These recent developments triggered renewed interest for the development of highly efficient fluorescent emitters for OLEDs. In this field, some of us pioneered the use of π-conjugated phospholes[6] such as **A–B** (Fig. 1) as purely fluorescent emitters for both colored and white OLEDs,[7] as well as for the development of hybrid-LEDs.[8] This P-based fluorophore takes advantage of an extended π-system and a trigonal P-atom limiting the stacking in the solid-state and, thus, promoting an intense solid-state luminescence. Furthermore, the specific reactivity in the P-atom also allows fine-tuning the emission wavelength.[9] Recently, the discovery of efficient metal-mediated synthesis of benzophospholes and the intense fluorescence associated with this core has led to the preparation of new libraries of fluorophores.[10] Among them, Tang *et al.* reported purely fluorescent OLEDs based on **C** (Fig. 1), which combine a strong electron donor (triarylamine) with the benzophosphole electron acceptor.[11] These devices displayed a satisfying efficiency with an EQE of 2%. In the present work, we report the synthesis of three new benzophosphole-based fluorophores having an ethoxy substituent on the P-atom (compounds **D** in Fig. 1) including different electron-donating groups, their full physico-chemical characterization based on a combined experimental–theoretical approach and their introduction in OLEDs. In particular, we show that one compound reaches an efficiency limit (EQE) of 5% for a purely fluorescent emitter, making it a very appealing derivative for further use in ultra-fast OLEDs or organic lasers.

Synthesis

The synthetic pathway to access fluorophores **2a–c** is illustrated in Scheme 1. The first step to obtain different arylamine-substituted

[a] Univ Rennes, CNRS, ISCR-UMR 6226, F-35000 Rennes, France
E-mail: pierre-antoine.bouit@univ-rennes.fr, muriel.hissler@univ-rennes.fr
[b] LPICM, CNRS, Ecole Polytechnique, Institut Polytechnique de Paris, route de Saclay, 91128 Palaiseau, France
[c] Université Paris-Saclay, CEA, CNRS, NIMBE, LICSEN, 91191, Gif-sur-Yvette, France
[d] Nantes Université, CNRS, CEISAM UMR 6230, F-44300, Nantes, France. E-mail: denis.jacquemin@univ-nantes.fr
[e] Institut Universitaire de France, F-75005 Paris, France

† Electronic supplementary information (ESI) available. See DOI: https://doi.org/10.1039/d3tc00245d

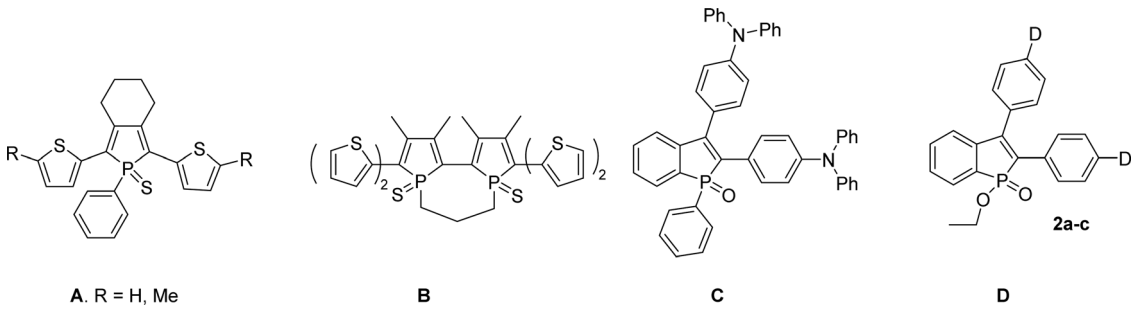

Fig. 1 Examples of phospholes (A)–(C) used as emitters in OLEDs and (D) the structure of the compounds considered in this study.

alkynes is based on a Hartwig-Buchwald reaction between 1,2-bis (4-bromophenyl)ethyne and the corresponding H-substituted arylamines. Then, benzophospholes were obtained by applying the procedure of Chen and coworkers,[10] that is using Ag_2O, ethyl phosphininate, and the corresponding alkynes *via* oxidative cyclization. Compounds **2a–c** were obtained in moderate yields between 31 and 40%. These compounds were fully characterized by multinuclear NMR spectroscopy, high-resolution mass spectrometry and elemental analyses (see the ESI†). In addition, they display good solubility in classical organic solvents.

Optical and redox properties

The spectroscopic properties of **2a–c** were investigated in diluted DCM solution (see Fig. 2A). All compounds display transitions in the UV-visible range up to 500 nm. **2a** and **2b** exhibit almost the same absorption properties with a first broad band around 300 nm. These two compounds also display a larger band in the visible range (λ_{max}(**2a**) = 406 nm; λ_{max}(**2b**) = 415 nm, see Table 1 and Fig. 2A). This large band is attributed to internal charge transfer (ICT) from the arylamine donor to the benzophosphole acceptor as it has been reported for similar compounds.[11] **2c** shows a maximal absorption wavelength at 327 nm and broad shoulder up to 480 nm (*vide infra* for theoretical rationalization).

2a and **2b** display fluorescence in diluted solution (DCM) with their maximum wavelengths at 578 nm and 637 nm, respectively (Fig. 2B and Table 1). A stronger redshift ($\Delta\lambda$ = 59 nm) is observed compared to the absorption, which is typical for molecules showing ICT. A solvent dependence study on **2a** indicates a positive solvatofluorochromism confirming the ICT nature of this transition (Fig. S13, ESI†). Both **2a** and **2b** show moderate photoluminescence quantum yields (PLQYs) of 0.34 and 0.09, respectively. This difference in PLQYs follows the energy-gap rule and is therefore unsurprising. **2c** does not luminesce in diluted DCM solution. All compounds display luminescence lifetime in the range of ns, typical of purely fluorescent emitters, even in degassed toluene (see the ESI†).

In the solid state, all derivatives display fluorescence emission, and their PLQY is enhanced compared to the diluted solution (Fig. 2C and Table 1). In powders, the emission wavelengths are blue-shifted compared to the solution, with maxima centered at 556 nm instead of 578 nm for **2a** and 610 nm instead of 637 nm for **2b**. **2a** even shows a PLQY of 1 in powder instead of 0.34 in the solution. This trend is the same when the PLQY is measured on thin films prepared by vacuum sublimation (Table 1). Interestingly, this value measured in the solid state is higher than the corresponding value of the analog molecule with an exocyclic phenyl moiety (PLQY = 0.68) instead of ethoxy.[11] It is clear that the modification of the phosphorus center can enhance the PLQY. **2b** displays a PLQY of 0.65 in powder, which is much higher than that in the solution (0.09). Interestingly, **2c**, which was poorly luminescent in solution, displays solid-state emission with a PLQY of 0.14. This enhancement of the emission in the solid state is known for related benzophosphole derivatives whose aggregation-induced emission (AIE) properties were already reported.[11]

The fluorescence lifetimes (τ) of these emitters were also measured at room temperature for the powder samples

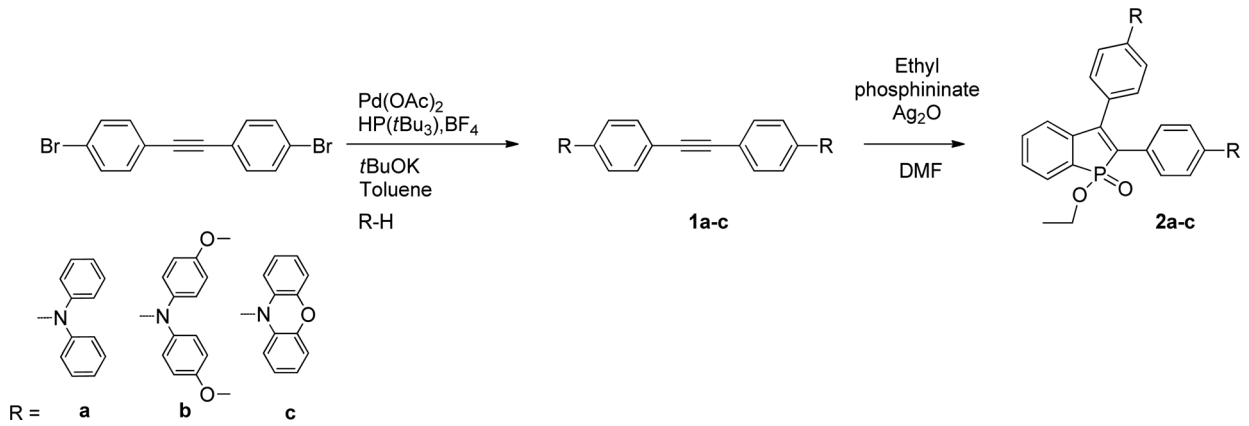

Scheme 1 Synthetic access to **2a–c**.

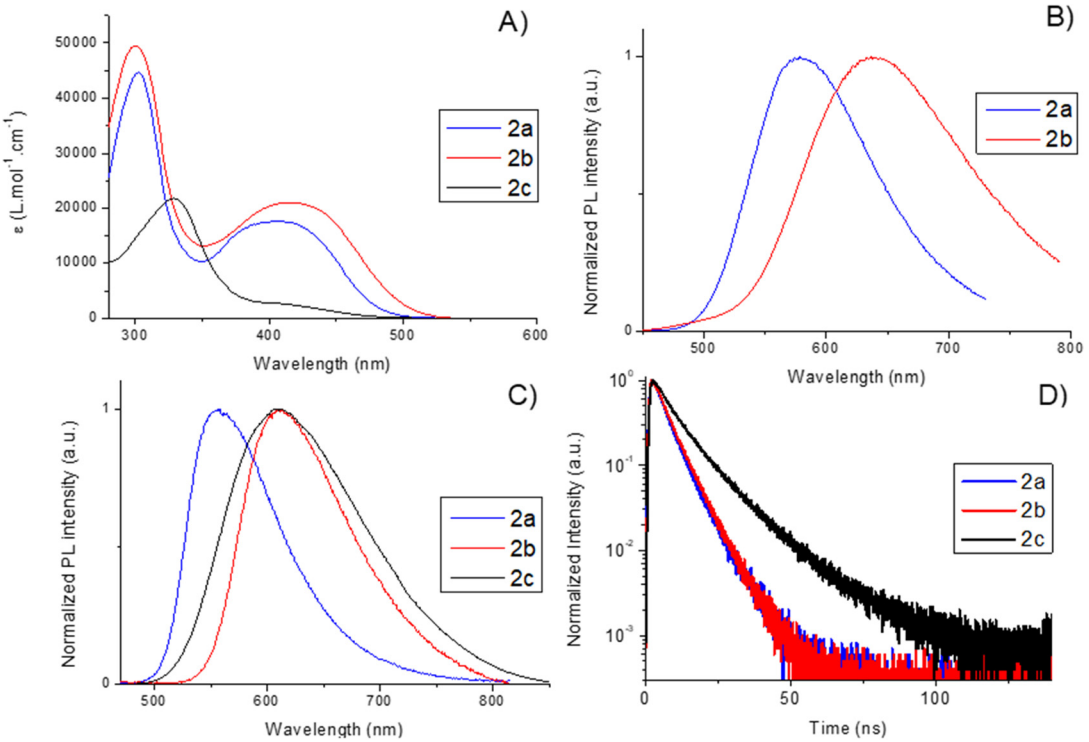

Fig. 2 (A) Absorption spectra of **2a–c** in DCM solution ($c \approx 1 \times 10^{-6}$ M). (B) Normalized emission spectra of **2a–c** in DCM solution ($c \approx 1 \times 10^{-6}$ M). (C) Normalized emission spectra of **2a–c** in powder. (D) Normalized transient PL decay of **2a–c** in powder.

Table 1 Photophysical data

	λ_{abs}[a] (nm)	ε[a] (L mol^{-1} cm^{-1})	λ_{em}[a] (nm)	Φ_{DCM}[b]	$\lambda_{em\ powder}$ (nm)	Φ_{powder}[c]	Φ_{film}[d]	τ (ns) powder	k_r[e] (10^7 s^{-1}) powder	k_{nr}[e] (10^7 s^{-1}) powder
2a	302, 406	45 000, 18 000	578	0.34	556	1	0.90	4.4(72%) 8.6(28%)	17.9	—
2b	301, 415	50 000, 21 000	637	0.09	610	0.65	0.54	4.7(61%) 7.6(39%)	11.1	6.0
2c	329, 410	22 000, 2600	—	—	609	0.14	0.16	6.3 (48%) 14.3(52%)	1.3	8.2

[a] In DCM solution (10^{-5} M). [b] Calculated relative to fluorescein (NaOH, 0.1 M), $\phi_{ref} = 0.79$. [c] Measured using a calibrated integration sphere. [d] Films prepared by vacuum sublimation. [e] k_r = radiative relaxation rate ($k_r = \Phi/\tau$); k_{nr} = non-radiative relaxation rate ($k_{nr} = (1 - \Phi)/\tau$).

(Fig. 2D and Table 1). All these emitters display a biexponential decay in the ns range, typical of fluorescence. This is in marked contrast to the TADF behavior observed using dibenzophosphole oxides substituted with similar amino groups,[12] highlighting the strong differences between benzophosphole and dibenzophosphole cores, as TADF has never been observed on substituted benzophospholes. The radiative (k_r) and non-radiative (k_{nr}) constants of these fluorophores have been calculated using their PLQY and the lifetime of their most contributive component. **2a** has a k_r value of 17.9×10^7 s^{-1} and no accurate value of k_{nr} can be given as the PLQY reaches 1. **2b** displays a lower k_r value of 11.1×10^7 s^{-1} and the appearance of a non-trifling k_{nr} of 6.0×10^7 s^{-1} reflecting the energy gap law. **2c** displays a considerably lower k_r value (1.3×10^7 s^{-1}), consistent with a small oscillator strength for the transition due to the poor conjugation between the donor and the acceptor driven by the twisted conformation of the phenoxazine group, as well as a rather large k_{nr} value (8.2×10^7 s^{-1}).

The electrochemical behavior of **2a–c** was investigated by cyclic voltammetry in DCM solution (Table 2 and Fig. S19–S23, ESI†). All three compounds display similar reduction processes, with the potential characteristic of the benzophosphole oxide unit: E_{red}(**2a**) = −1.59 V *vs.* FeCp*$_2^{+/0}$, E_{red}(**2b**) = −1.70 V *vs.* FeCp*$_2^{+/0}$ and E_{red}(**2c**) = −1.46 V *vs.* FeCp*$_2^{+/0}$. Moreover, **2a** and **2b** display an irreversible process for the reduction while **2c** shows a quasi-reversible process. Regarding oxidation, all compounds display oxidation waves typical of arylamines. These processes are quasi-reversible for **2a** and **2b**, and reversible for **2c**. All the oxidation waves are doubled in intensity compared to the reductions, due to the presence of two arylamine groups. The values of E_{ox} nicely reflect the electron-donating ability of different amines: E_{ox} (**2a**) = +1.06 V *vs.* FeCp*$_2^{+/0}$, E_{ox} (**2b**) = +0.83 V *vs.* FeCp*$_2^{+/0}$ and E_{ox} (**2c**) = +0.87 V *vs.* FeCp*$_2^{+/0}$.

To gain deeper insights into the optical properties of the fluorophores, DFT and TD-DFT calculations were carried out (see the ESI† for details). By considering the various systems, a

Table 2 Redox data[a]

	E_{ox} (V *vs.* $FeCp^*_2{}^{+/0}$)	E_{red} (V *vs.* $FeCp^*_2{}^{+/0}$)	HOMO[b] (eV)	LUMO[b] (eV)	E_g redox (eV)	E_g optical (eV)
2a	+1.06	−1.59	−5.21	−2.74	2.47	2.58
2b	+0.83	−1.70	−4.97	−2.64	2.33	2.48
2c	+0.87	−1.46	−5.06	−2.86	2.20	2.58

[a] ($c = 10^{-3}$ M) recorded in CH_2Cl_2 with $Bu_4N^+PF_6^-$ (0.2 M) at a scan rate of 200 mV s^{-1}. [b] HOMO (eV) = $-E_{ox}$(onset) (−4.8 + 0.545)//LUMO (eV) = $-E_{red}$(onset) (−4.8 + 0.545). *E* (1/2)$FeCp_2^{+/0}$ *vs.* $FeCp^*_2{}^{+/0}$ in DCM = 0.545 V.[13,14]

notable difference appears in absorption. Indeed, while for **2a** and **2b**, TD-DFT yields a strongly dipole-allowed first transition with respective *f* larger than 0.400, the two first excitations of **2c** show very weak oscillator strengths of 0.027 and 0.017, and it is only the third transition that develops a sizeable *f* (0.317) in this compound. The computed vertical absorptions for the first transition are 402 and 415 for **2a** and **2b**, respectively. Although the vertical absorption values are not λ_{max},[14] one can see a reasonable qualitative match between experiment and theory in terms of the position of the first strong absorption. For **2c**, the two weakly allowed transitions are positioned at 374 and 367 nm, and the main strong band at 324 nm. This is well in line with the experimental finding: a strong absorption between 300 and 350 nm, followed by a long tail at longer wavelengths for **2c** (Fig. 2A).

In Fig. 3, we illustrate the lowest excited states of **2a** and **2b**. The topology of these transitions is obviously similar, with NPh_2 units acting as donor groups and the P-containing core of the dye acting as the acceptor. The ICT seems a bit stronger in the group located at the 2-position of phosphole, whereas the impact of methoxy substituents is rather limited, which is unsurprising given the already strong donating character of the NPh_2 groups.

Let us now focus on **2c**, see Fig. 4: the two weakly allowed transitions correspond to pure ICT states from phenoxazine to the dye core, but the almost perpendicular nature of the two π-conjugated (sub)systems makes these absorptions nearly dark. The strong absorption at higher energy is localized on the dye core. This means that the difference in absorption spectra between the various dyes is mainly a consequence of the geometrical constraints: while diphenylamine is electronically connected to the P-bearing cycles thanks to its propeller shape, the orthogonality of phenoxazine cuts such direct connection and only through-space ICT takes place.

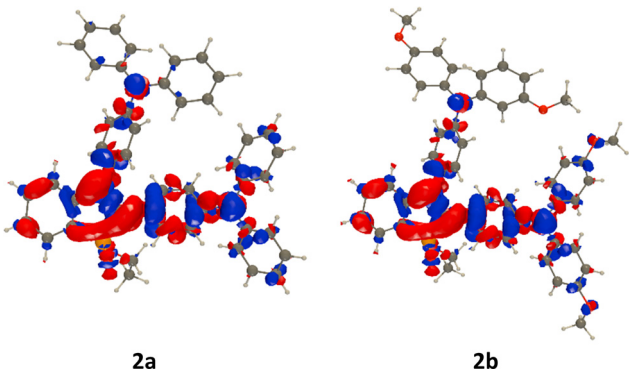

Fig. 3 Electron density difference (EDD) plots for the lowest excited states of **2a** and **2b**. The blue and red regions correspond to the decrease and increase of density upon excitation, respectively. Contour threshold: 0.001 au.

We have determined the 0–0 energies of the three emissive dyes in the solution; as these can be straightforwardly compared between experiment and theory, we obtained the following values: 481 nm (**2a**) and 495 nm (**2b**), which are close to the experimental absorption–emission crossing point, with a +14 nm redshift between **2a** and **2b**, also fitting experiment (+17 nm). These results confirm the robustness of the selected theoretical level.

Finally, theoretical calculations were performed to determine the singlet–triplet (S–T) gaps at the optimal S1 geometries of **2a**, **2b**, and **2c** (see the ESI† for details). For **2a**, only one triplet state is lower than the S1 state, with a large gap of 0.73 eV. The results are similar for both **2b** and **2c**, with respective S1–T1 gaps of 0.71 eV and 0.66 eV, respectively. This indicates an unfavorable situation for TADF to appear, in full agreement with the experimental observations.

OLED devices

Taking advantage of the excellent luminescence properties of **2a–c** and their high thermal stability (325 °C < T_d(**2a–c**) < 330 °C), compounds **2a–c** were introduced as emitters into multilayered OLED devices (see the ESI† for details). Because of their suitable HOMO–LUMO levels and their high solid-state luminescence, **2a–c** were used as pure emitters and inside a host 4,4-bis(2,2-diphenylvinyl)-1,1-diphenyl (DPVBi) matrix. The performances of the OLED devices are reported in Table 3 for **2a–c** used as pure emitters or at a doping ratio of 5% in the DPVBi matrix. This doping ratio of 5% has been set after a study of EQE *vs.* doping ratio on **2a** (see Fig. S24, ESI†).

All emitters display blue-shifted electroluminescence compared to the photoluminescence in the solid state. This blue shift is even stronger when these emitters are used in the DPVBi matrix: λ_{max}EL (**2a** 5% in dPVBi) = 532 nm; λ_{max}EL (**2a** pure) = 552 nm; λ_{max}em (**2a** powder) = 556 nm. As DPVBi is an apolar matrix (Fig. S25, ESI†), this hypsochromic shift was expected. In all cases, the values of EQE follow the trend of the PLQY of the emitters in powder: EQE(**2c**) < EQE(**2b**) < EQE(**2a**). The theoretical value of 5% EQE for a fluorescent OLED is even reached with compound **2a** in device **A**. It should be noted that such a theoretical limit of EQE is calculated for an outcoupling efficiency of 20%. However, the outcoupling might be higher by horizontal orientations of the emissive transition dipole moment.[15] Moreover, device **A** displays a small roll-off efficiency illustrated by its very high brightness of 27 010 cd m^{-2} at a high current density of 220 mA cm^{-2}. These values represent a considerable increase compared to the previously reported related compounds and thus highlight the dramatic impact of small molecular variations on the properties of the device.[11,16]

Devices containing pure emitters in the emissive layer exhibit less efficient properties than devices containing DPVBi

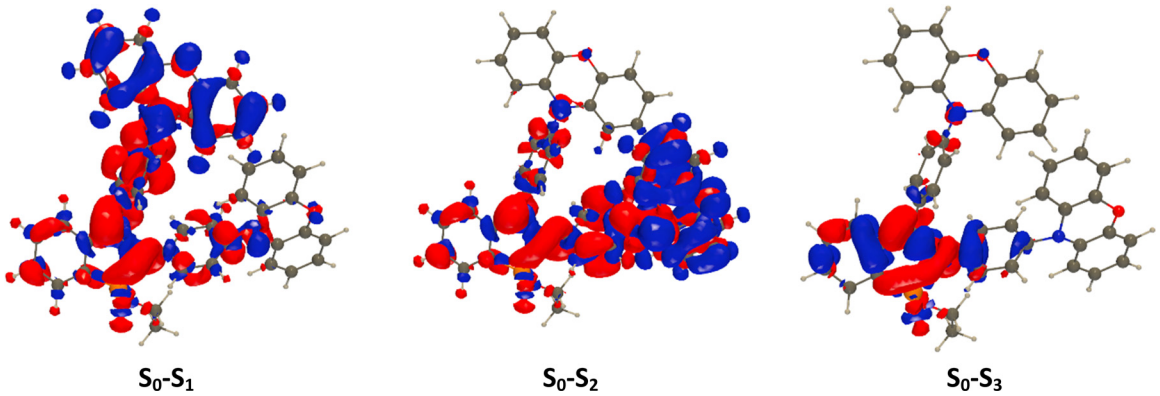

Fig. 4 Electron density difference (EDD) plots for the three lowest excited state of **2c**.

Table 3 Device characteristics

Device	Emitter	Doping ratio (%)	V_{on}[a] (V)	EQE[b] (%)	λ_{max} EL (nm)	CE[b] (cd A^{-1})	PE[b] (lm W^{-1})	Maximal brightness (cd m^{-2}) (@mA cm^{-2})
A	**2a**	5	3.7	5.1	532	17.06	8.20	27 010 (220)
B	**2b**	5	3.6	4.2	556	14.28	6.86	19 200 (200)
C	**2c**	5	4.2	2.3	556	6.42	2.75	5958 (140)
D	**2a**	Pure	2.8	3.6	552	13.55	7.98	17 500 (300)
E	**2b**	Pure	2.6	2.0	588	5.30	3.38	8586 (340)
F	**2c**	Pure	3.4	0.8	588	1.52	0.90	3600 (340)

[a] Recorded at a luminance of 0.1 cd m^{-2}. [b] External quantum efficiency, current efficiency (CE) and power efficiency (PE) recorded at 30 mA cm^{-2}.

(EQE(**A**) = 5.1%; EQE(**D**) = 3.6%). Interestingly, the V_{on} values of devices **D**, **E**, and **F** are significantly lower than those of devices **A**, **B**, and **C** (by *ca.* 1 V), indicating that the injection of charge inside the emissive layer is easier when there is no DPVBi. This property leads to better stability of devices **D**, **E**, and **F**: the maximal brightness is reached at a higher value of current density (300 to 340 mA cm^{-2}) than that of devices **A**, **B**, and **C** (140 to 220 mA cm^{-2}). To rationalize the difference of EQE, the photoluminescence of emissive layers (deposited on a glass substrate using evaporation) was studied (Table S2, ESI†). DPVBi has almost no impact on the PLQY of **2a** (Φ_{PL}(5% in DPVBi) = 0.93 and Φ_{PL}(pure) = 0.90) while the impact on **2b** and **2c** is much larger (Φ_{PL}(**2b** 5% in dPVBi)= 0.85; Φ_{PL}(**2b** pure) = 0.54; Φ_{PL}(**2c** 5% in DPVBi) = 0.36; Φ_{PL}(**2c** pure) = 0.16). This effect is related to the ICT character of the emissive transition of **2a–c**: the apolar environment of DPVBI enhances the contribution of the locally excited state, higher in energy and more emissive than the ICT state. Such behavior explains both the hypsochromic shift and the higher EQE for devices **A**, **B** and **C** using a host matrix.

Conclusions

In this article, we report the synthesis and full characterization of a family of benzophopsholes **2a–c** substituted by electrodonating amino groups. The nature of the donor allows fine-tuning the ICT and thus the optical properties. In particular, these compounds display intense fluorescence in the solid state (powders/thin films). Considering the favorable redox and thermal properties, the compounds were introduced in multilayered OLED devices displaying high EQE reaching 5% for compound **2a**. This is indeed the theoretical limit of the efficiency of purely fluorescent emitters. Ethoxy-substituted benzophopshole oxides thus represent a new class of highly efficient emitters for OLEDs. The introduction of these emitters into organic lasers or fast OLEDs will be investigated in the future.

Conflicts of interest

There are no conflicts to declare.

Acknowledgements

This work was supported by the Ministère de la Recherche et de l'Enseignement Supérieur, the CNRS, the Région Bretagne, the French National Research Agency (ANR Fluohyb ANR-17-CE09-0020) and the China-French associated international laboratory in ''Functional Organophosphorus Materials'', the GDR Phosphore. NL thanks the Région Bretagne for PhD grant. PAB thanks C. Quinton for assistance with lifetime measurements. DJ is indebted to the CCIPL computational center installed in Nantes for generous allocation of computational time.

References

1 C. W. Tang and S. A. VanSlyke, *Appl. Phys. Lett.*, 1987, **51**, 913.

2 (*a*) K. Müllen and U. Scherf, *Organic Light Emitting Devices*, Wiley-VCH, Weinheim, 2006; (*b*) B. Geffroy, P. Le Roy and C. Prat, *Polym. Int.*, 2006, **55**, 572; (*c*) G. Hong, X. Gan, C. Leonhardt, Z. Zhang, J. Seibert, J. M. Busch and S. Bräse, *Adv. Mater.*, 2021, **33**, 2005630.

3 (*a*) H. Nakanotani, T. Higuchi, T. Furukawa, K. Masui, K. Morimoto, M. Numata, H. Tanaka, Y. Sagara, T. Yasuda and C. Adachi, *Nat. Commun.*, 2014, **5**, 4016; (*b*) M. Cai, D. Zhang and L. Duan, *Chem. Rec.*, 2019, **19**, 1611.

4 (*a*) A. S. D. Sandanayaka, T. Matsushima, F. bencheickh, S. Terakawa, W. J. Postcavage Jr, C. Qin, T. Fujihara, K. Goushi, J. C. Ribierre and C. Adachi, *Appl. Phys. Express*, 2019, **12**, 061010; (*b*) Q. Zhang, W. Tao, J. Huang, R. Xia and J. Cabanillas-Gonzalez, *Adv. Photonics Res.*, 2021, **2**, 2000155.

5 K. Yoshida, P. P. Manousiadis, R. Bian, Z. Chen, C. Murawski, M. C. Gather, H. Haas, G. A. Turnbull and I. D. W. Samuel, *Nat. Commun.*, 2020, **11**, 1171.

6 (*a*) F. Mathey, *Chem. Rev.*, 1988, **88**, 429; (*b*) R. Réau and T. Baumgartner, *Chem. Rev.*, 2006, **106**, 4691; (*c*) Y. Matano and H. Imahoria, *Org. Biomol. Chem.*, 2009, **7**, 1258.

7 (*a*) C. Fave, T. Y. Cho, M. Hissler, C. W. Chen, T. Y. Luh, C. C. Wu and R. Réau, *J. Am. Chem. Soc.*, 2003, **125**, 9254; (*b*) O. Fadhel, M. Gras, N. Lemaitre, V. Deborde, M. Hissler, B. Geffroy and R. Réau, *Adv. Mater.*, 2009, **21**, 1261; (*c*) H. Chen, W. Delaunay, L. Yu, D. Joly, Z. Wang, J. Li, Z. Wang, C. Lescop, D. Tondelier, B. Geffroy, Z. Duan, M. Hissler, F. Mathey and R. Réau, *Angew. Chem., Int. Ed.*, 2012, **51**, 214; (*d*) C. Romero-Nieto, M. Marcos, S. Merino, J. Barbera, T. Baumgartner and J. Rodriguez-Lopez, *Adv. Funct. Mater.*, 2011, **21**, 4088.

8 (*a*) J. Phelipot, N. Ledos, T. Dombray, M. P. Duffy, M. Denis, T. Wang, Y. Didane, M. Gaceur, Q. Bao, X. Liu, M. Fahlman, P. Delugas, A. Mattoni, D. Tondelier, B. Geffroy, P.-A. Bouit, O. Margeat, J. Ackermann and M. Hissler, *Adv. Mater. Technol.*, 2022, 2100876; (*b*) J. Kuno, N. Ledos, P.-A. Bouit, T. Kawai, M. Hissler and T. Nakashima, *Chem. Mater.*, 2022, **34**, 9111–9118; (*c*) J. Phelipot, P. Manzhi, N. Ledos, D. Tondelier, B. Geffroy, P.-A. Bouit, J. Ackermann, M. Hissler and O. Margeat, *New J. Chem.*, 2022, **46**, 22574–22580.

9 M. Duffy, W. Delaunay, P.-A. Bouit and M. Hissler, *Chem. Soc. Rev.*, 2016, **45**, 5296.

10 (*a*) Y.-R. Chen and W. -L. Duan, *J. Am. Chem. Soc.*, 2013, **135**, 16754; (*b*) Y. Unoh, K. Hirano, T. Satoh and M. Miura, *Angew. Chem., Int. Ed.*, 2013, **52**, 12975; (*c*) V. Quint, F. Morlet-Savary, J.-F. Lohier, J. Lalevée, A.-C. Gaumont and S. Lakhdar, *J. Am. Chem. Soc.*, 2016, **138**, 7436–17441; (*d*) C. Wang, A. Fukazawa, M. Taki, Y. Sato, T. Higashiyama and S. Yamaguchi, *Angew. Chem., Int. Ed.*, 2015, **127**, 15428.

11 Z. Zhuang, F. Bu, W. Luo, H. Peng, S. Chen, R. Hu, A. Qin, Z. Zhao and B. Z. Tang, *J. Mater. Chem. C*, 2017, **5**, 1836.

12 J. I. Nishida, Y. Kawakami, S. yamamoto, Y. Matsui, H. Ikeda, Y. Hirao and T. Kawase, *Eur. J. Org. Chem.*, 2019, 3735.

13 J. R. Aranzaes, M. C. Daniel and D. Astruc, *Can. J. Chem.*, 2006, **84**, 288.

14 A. D. Laurent, C. Adamo and D. Jacquemin, *Phys. Chem. Chem. Phys.*, 2014, **16**, 14334.

15 F. Tenopala-Carmona, O. S. Lee, E. Crovini, A. M. Neferu, C. Murawski, Y. Olivier, E. Zysman-Colman and M. C. Gather, *Adv. Mater.*, 2021, **33**, 2100677.

16 In addition to the structural change in the emitter, the structure of the OLED stack also slightly differs, see ref. 11.